

Unpolarized Transverse-Momentum-Dependent Parton Distributions of the Nucleon from Lattice QCD (Lattice Parton Collaboration (LPC))



Jin-Chen He,^{1,2,3} Min-Huan Chu,^{1,2} Jun Hua,^{4,5} Xiangdong Ji,³ Andreas Schäfer,⁶
Yushan Su,³ Wei Wang,^{2,*} Yi-Bo Yang,^{7,8,9,10} Jian-Hui Zhang,^{11,12} and Qi-An Zhang^{13,†}

¹*Yang Yuanqing Scientific Computing Center, Tsung-Dao Lee Institute,
Shanghai Jiao Tong University, Shanghai 200240, China*

²*Shanghai Key Laboratory for Particle Physics and Cosmology,
Key Laboratory for Particle Astrophysics and Cosmology (MOE),
School of Physics and Astronomy, Shanghai Jiao Tong University, Shanghai 200240, China*

³*Department of Physics, University of Maryland, College Park, MD 20742, USA*

⁴*Guangdong Provincial Key Laboratory of Nuclear Science, Institute of Quantum Matter,
South China Normal University, Guangzhou 510006, China*

⁵*Guangdong-Hong Kong Joint Laboratory of Quantum Matter,
Southern Nuclear Science Computing Center, South China Normal University, Guangzhou 510006, China*

⁶*Institut für Theoretische Physik, Universität Regensburg, D-93040 Regensburg, Germany*

⁷*CAS Key Laboratory of Theoretical Physics, Institute of Theoretical Physics,
Chinese Academy of Sciences, Beijing 100190, China*

⁸*School of Fundamental Physics and Mathematical Sciences,
Hangzhou Institute for Advanced Study, UCAS, Hangzhou 310024, China*

⁹*International Centre for Theoretical Physics Asia-Pacific, Beijing/Hangzhou, China*

¹⁰*School of Physical Sciences, University of Chinese Academy of Sciences, Beijing 100049, China*

¹¹*School of Science and Engineering, The Chinese University of Hong Kong, Shenzhen 518172, China*

¹²*Center of Advanced Quantum Studies, Department of Physics,
Beijing Normal University, Beijing 100875, China*

¹³*School of Physics, Beihang University, Beijing 102206, China*

We present a first calculation of the unpolarized proton's isovector transverse-momentum-dependent parton distribution functions (TMDPDFs) from lattice QCD, which are essential to predict observables of multi-scale, semi-inclusive processes in the standard model. We use a $N_f = 2 + 1 + 1$ MILC ensemble with valence clover fermions on a highly improved staggered quark sea (HISQ) to compute the quark momentum distributions in large-momentum protons on the lattice. The state-of-the-art techniques in renormalization and extrapolation in correlation distance on the lattice are adopted. The one-loop contributions in the perturbative matching kernel to the light-cone TMDPDFs are taken into account, and the dependence on the pion mass and hadron momentum is explored. Our results are qualitatively comparable with phenomenological TMDPDFs, which provide an opportunity to predict high energy scatterings from the first principles.

Introduction: Since the nucleon is at the core of the atoms and accounts for nearly all of the mass of the visible universe, exploring its internal structure has been a key task for more than a century in both particle and nuclear physics. In high-energy scattering, the quark and gluon transverse momentum and polarization degrees of freedom in the nucleon are best described by transverse-momentum parton distribution functions (TMDPDFs). Thus, mapping out the nucleon's TMDPDFs is a crucial step in understanding the interactions between quarks and gluons, and possibly the phenomena of confinement [1, 2]. Moreover, predicting the observables in multi-scale, non-inclusive high energy processes such as semi-inclusive deep-inelastic scattering and Drell-Yan scattering at the large hadron collider (LHC) or elec-

tron ion collider (EIC) heavily relies on the knowledge of TMDPDFs [3, 4].

Whereas high energy experiments have accumulated a wealth of relevant data, our knowledge of TMDPDFs is far from being complete. Their rapidity evolution, i.e. Collins-Soper kernel [1], has been perturbatively calculated up to four loops [5], but TMDPDFs at low energies are nonperturbative in nature. Based on thousands of data points from the low- p_T semi-inclusive DIS and Drell-Yan scattering processes and perturbative-QCD factorization, a number of phenomenological analyses have been made to obtain state-of-art TMDPDFs [6–9]. Although similar sets of data have been used in these analyses, the results however differ significantly from each other. It indicates that significant uncertainties exist

in the global extraction of TMDPDFs, and further constraints are necessary for a refined determination.

First-principles calculations of TMDPDFs require non-perturbative methods such as lattice QCD. A handful of available investigations on lattice QCD are limited to ratios of moments of TMDPDFs [10–13]. The development of large momentum effective theory (LaMET) allows the extraction of light-cone quantities through the simulation of equal-time quasi distributions [14, 15]. A direct generalization of this essence to calculating TMDPDFs is non-trivial due to the presence of soft function [16], which involves two opposite light-like directions and presents a crucial difficulty to implement on a Euclidean lattice. A recent progress demonstrates that the rapidity-independent (intrinsic) soft function can be calculated from a large-momentum-transfer form factor of a light meson [17], while the rapidity evolution kernel in soft function can be accessed via the quasi TMDPDFs/beam functions [16, 18–20] or quasi transverse-momentum-dependent wave functions [17, 21]. Subsequent lattice efforts have been devoted to explore the Collins-Soper kernel and intrinsic soft function, and the agreement between lattice results and phenomenological analyses is encouraging [19, 22–25].

Following these developments, this work presents a first calculation of TMDPDFs from the first principles of strong interactions. We simulate the TMD momentum distributions in a large momentum nucleon or quasi TMDPDFs on the lattice and perform a systematic study of renormalization property by considering the subtractions from Wilson loop combined with the short distance hadron matrix element [27]. In the matching from quasi TMDPDFs, we include one-loop perturbative contributions and employ the renormalization group equation to resum the logarithms. After analyzing the pion mass and momentum dependence, our final results for TMDPDFs are found to have a similar behavior to the phenomenological fits.

Theoretical framework: Describing the momentum distributions of a parton inside a hadron, TMDPDFs $f(x, b_\perp, \mu, \zeta)$ are functions of longitudinal momentum fraction x , the Fourier conjugate b_\perp of the parton transverse momentum q_\perp , as well as the renormalization scale μ and rapidity scale ζ . In this work we will consider the flavor non-singlet/isovector unpolarized quark TMDPDFs, which are free from the mixing with gluons.

In LaMET, the correlations with modes traveling along the light-cone can be extracted from distributions in a fast-moving nucleon through large-momentum expansion. On the lattice, the equal-time quasi TMDPDFs are constructed as

$$\tilde{f}_\Gamma(x, b_\perp, P^z, \mu) \equiv \lim_{\substack{a \rightarrow 0 \\ L \rightarrow \infty}} \int \frac{dz}{2\pi} e^{-iz(xP^z)} \times \frac{\tilde{h}_\Gamma^0(z, b_\perp, P^z, a, L)}{\sqrt{Z_E(2L+z, b_\perp, a)} Z_O(1/a, \mu, \Gamma)}, \quad (1)$$

in which a denotes the lattice spacing. $\Gamma = \gamma^t$ or γ^z is the Dirac matrix that can be projected onto γ^+ in the large momentum limit. Differences between the two choices might reveal the magnitude of power corrections. The $\tilde{h}_\Gamma^0(z, b_\perp, P^z, a, L)$ is built with a gauge-invariant nonlocal quark bilinear operator as

$$\tilde{h}_\Gamma^0(z, b_\perp, P^z, a, L) = \langle P^z | \tilde{O}_{\Gamma, \square}^0(z, b_\perp, P^z; L) | P^z \rangle \quad (2)$$

$$\tilde{O}_{\Gamma, \square}^0(z, b_\perp, L) \equiv \bar{\psi}(b_\perp \hat{n}_\perp) \Gamma U_{\square, L}(b_\perp \hat{n}_\perp, z \hat{n}_z) \psi(z \hat{n}_z) \quad (3)$$

In the equations above, $|P^z\rangle$ denotes the unpolarized proton state and L corresponds to the farthest distance that the gauge link can reach in positive or negative \hat{n}_z direction on a finite Euclidean lattice. The staple-shaped Wilson link is chosen as

$$U_{\square, L}(b_\perp \hat{n}_\perp, z \hat{n}_z) \equiv U_z^\dagger(L \hat{n}_z + b_\perp \hat{n}_\perp, b_\perp \hat{n}_\perp) \times U_\perp(L \hat{n}_z + b \hat{n}_\perp, L \hat{n}_z) U_z(L \hat{n}_z, z \hat{n}_z), \quad (4)$$

with the path-ordered Euclidean gauge links along the z -direction connecting at the “infinity” position L . The staple-shaped Wilson link is depicted as double lines in Fig. 1.

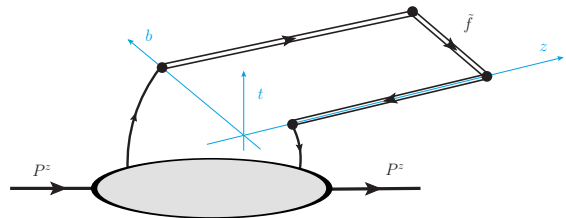


FIG. 1. Illustration of the unstuctured quasi TMDPDFs.

Quantities in Eq. (2) and (3) with the superscript “0” are bare quantities on a finite lattice. They contain linear divergence, pinch-pole singularity and logarithm divergence. Both the linear divergence that comes from the self-energy corrections of Wilson line and the pinch-pole singularity from interactions between the two Wilson lines along the z direction can be renormalized by the square root of Wilson loop $\sqrt{Z_E(2L+z, b_\perp, a)}$ [28–32]; and the logarithm divergence comes from the vertices involving Wilson line and light quark, and can be renormalized by $Z_O(1/a, \mu)$ with $\overline{\text{MS}}$ -scale μ [27, 33–35]. More details are given in the supplemental material [36].

It has been shown that quasi TMDPDFs have the same collinear degree of freedoms with TMDPDFs [20]. Their differences from soft modes can be attributed to the intrinsic soft function and different rapidity scales, and meanwhile contributions from highly off-shell modes are local [18]. Thus TMDPDFs $f(x, b_\perp, \mu, \zeta)$ can be connected with quasi TMDPDFs $\tilde{f}_\Gamma(x, b_\perp, \zeta_z, \mu)$ via a multiplicative factorization [20, 37]:

$$\tilde{f}_\Gamma(x, b_\perp, \zeta_z, \mu) \sqrt{S_I(b_\perp, \mu)} = H_\Gamma \left(\frac{\zeta_z}{\mu^2} \right) e^{\frac{1}{2} \ln(\frac{\zeta_z}{\mu^2}) K(b_\perp, \mu)}$$

$$\times f(x, b_\perp, \mu, \zeta) + \mathcal{O}\left(\frac{\Lambda_{\text{QCD}}^2}{\zeta_z}, \frac{M^2}{(P^z)^2}, \frac{1}{b_\perp^2 \zeta_z}\right), \quad (5)$$

where S_I is the intrinsic soft function [17], and K is Collins-Soper kernel. The matching kernel $H_\Gamma = e^h$ is a function of $\zeta_z/\mu^2 = (2xP^z)^2/\mu^2$ and same for the γ^t and γ^z . The one-loop result $h^{(1)}$ has been calculated in Ref. [20] and collected in the supplemental material [36]. The logarithms in ζ_z/μ^2 are summed using renormalization group equation. Power corrections are suppressed by $\mathcal{O}\left(\Lambda_{\text{QCD}}^2/\zeta_z, M^2/(P^z)^2, 1/(b_\perp^2 \zeta_z)\right)$, which implies that only in the moderate x region TMDPDFs can be reliably extracted.

Lattice simulations: We use the valence tadpole improved clover fermion on the hypercubic (HYP) smeared [38] 2+1+1 flavors MILC configurations with highly improved staggered quark (HISQ) sea and 1-loop Symanzik improved gauge action [39]. This calculation adopts a single ensemble with lattice spacing $a = 0.12$ fm and volume $n_s^3 \times n_t = 48^3 \times 64$ using physical sea quark masses, and uses two choices of light valence quark mass corresponding to $m_\pi^{\text{val}} = 310$ MeV and 220 MeV. The HYP smearing is also used for nonlocal correlation functions to improve the statistical signal. In order to explore the momentum dependence, we employ three different nucleon momenta as $P^z = 2\pi/(n_s a) \times \{8, 10, 12\} = \{1.72, 2.15, 2.58\}$ GeV.

We adopt momentum-smearing point source [40] at several time slices, and average correlation functions for both the forward and backward directions in z and transverse space of the gauge link. In total, there are 1000 (cfg.) $\times 16$ (source time slices) $\times 4$ (forward/backward directions of the z and transverse axes) measurements for the $m_\pi^{\text{val}} = 220$ MeV case and $1000 \times 4 \times 4$ measurements for the 310 MeV case.

To extract the quasi TMDPDFs, one can construct the two point functions (2pt) as well as three point functions (3pt) as

$$C_2(t) = \left\langle \sum_{\vec{y}} e^{i\vec{P}\cdot\vec{y}} T_{\text{unpol}} \chi(\vec{y}, t) \bar{\chi}(\vec{0}, 0) \right\rangle, \quad (6)$$

$$C_3^\Gamma(t, t_{\text{seq}}) = \left\langle \sum_{\vec{y}} e^{i\vec{P}\cdot\vec{y}} T_{\text{unpol}} \chi(\vec{y}, t_{\text{seq}}) \times \left(\sum_{\vec{x}} \tilde{O}_{\text{nonlocal}}^\Gamma(\vec{x}, t) \right) \bar{\chi}(\vec{0}, 0) \right\rangle, \quad (7)$$

where $T_{\text{unpol}} = (1 + \gamma^t)/2$ is the unpolarized projector, and $\chi = \epsilon^{abc} u_a (u_b^T C \gamma_5 d_c)$ is the nucleon interpolation field. We adopt the sequential source method [41] to reduce the number of propagators in 3pt, and t_{seq} denotes the time position of sequential source. The operator $\tilde{O}_{\text{nonlocal}}^\Gamma(\vec{x}, t)$ is short for the TMD nonlocal quark bilinear operator $\tilde{O}_{\square}^0(\vec{x} + z\hat{n}_z, \vec{x} + b_\perp \hat{n}_\perp, \Gamma, L)$ at discrete time slice $t \in [0, t_{\text{seq}}]$. The three-momentum is chosen as $\vec{P} = (0, 0, P^z)$.

For a well-defined quasi TMDPDF, the length of Wilson link L should be large enough to ensure the independence of final results on L . Ref. [27] has systematically analyzed the L -dependence of quasi TMDPDF operators on different gauge configurations. Following these investigations we adopt $L = 6a$ as the saturated length of Wilson link.

After interpolating the single particle intermediate states, the ratio of $C_3^\Gamma(t, t_{\text{seq}})$ and $C_2(t_{\text{seq}})$ becomes

$$\frac{C_3^\Gamma(t, t_{\text{seq}})}{C_2(t_{\text{seq}})} = \frac{\tilde{h}_\Gamma^0 + c_2(e^{-\Delta E t} + e^{-\Delta E(t_{\text{seq}} - t)}) + c_3 e^{-\Delta E t_{\text{seq}}}}{1 + c_1 e^{-\Delta E t_{\text{seq}}}}, \quad (8)$$

in which $\tilde{h}_\Gamma^0 \equiv \tilde{h}^0(z, b_\perp, P^z, \Gamma)$, ΔE is the mass gap between the ground-state and excited state, and $c_{1,2,3}$ are parameters for the excited-state contamination. Combing the parametrization form of 2pt: $C_2(t) = c_0 e^{-E_0 t} (1 + c_1 e^{-\Delta E t})$, one can extract the values of \tilde{h}_Γ^0 at fixed (z, b_\perp, P^z) through a joint fit. The ratios with different t_{seq} and t at $\{z, b_\perp, P^z\} = \{3a, 1a, 16\pi/n_s\}$ and $\Gamma = \gamma^t$, $m_\pi = 220$ MeV case are shown in Fig. 8 of the supplemental material [36]. In this example, a satisfactory fit with $\chi^2/\text{d.o.f} = 0.95$ is obtained in the fit range $t \in [1, t_{\text{seq}} - 1]a$, and all the other cases are similar with good fitting qualities ($\chi^2/\text{d.o.f} \sim 1$ and p -value > 0.1).

Combing the bare quasi TMDPDFs matrix elements, the corresponding Wilson loop and renormalization factor in the supplemental material [36], we obtain numerical results for renormalized matrix elements at different $\lambda = zP^z$. The left panels in Fig. 2 exhibit the λ dependence of quasi TMDPDFs with $b_\perp = 3a$ with various P^z and m_π . From these panels, the quasi TMDPDFs approach zero at large λ for both real and imaginary parts, which ensures the convergence and smoothness of quasi TMDPDFs in momentum space. For the cases with large b_\perp and P^z , uncertainties in the data become sizably large, as shown in the right panels in Fig. 2 with $b_\perp = 5a$ and $P^z = 1.72\text{GeV}$. To limit the uncertainty and augment the lattice data at large z , we adopt an extrapolation at large λ with the form: [31]

$$\tilde{h}_{\Gamma, \text{extra}}(\lambda) = \left[\frac{m_1}{(-i\lambda)^{n_1}} + e^{i\lambda} \frac{m_2}{(i\lambda)^{n_2}} \right] e^{-\lambda/\lambda_0}, \quad (9)$$

in which all the parameters $m_{1,2}$, $n_{1,2}$ and λ_0 depend on the transverse separation b_\perp . The algebraic terms account for a power law behavior of TMDPDFs in the endpoint region, and the exponential term comes from the expectation that the correlation function has a finite correlation length (denoted as λ_0) [31] at finite momentum, which becomes infinite when the momentum goes to infinity.

In practice, a reasonable region in λ is required to determine the extrapolation parameters. We choose the data points with $z \geq 8a$ for the extrapolation, and use the region with $z \geq 6a$ to estimate the systematic errors.

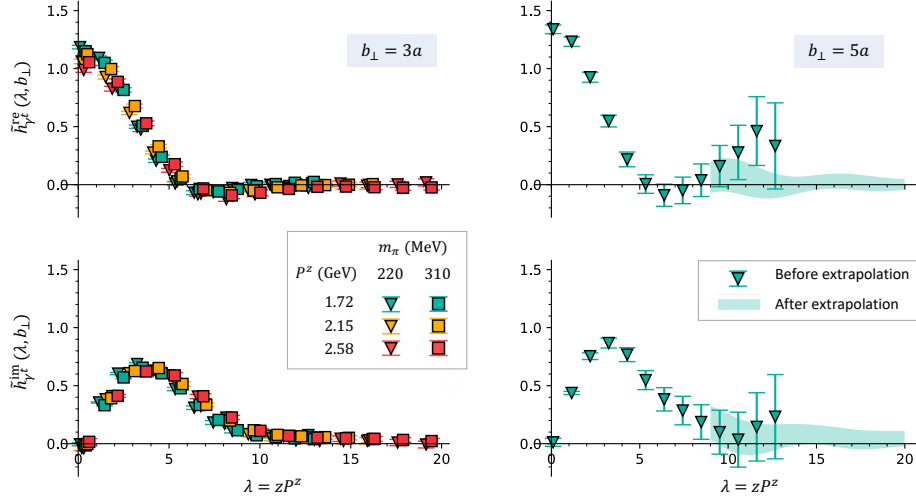


FIG. 2. Left panels: the renormalized quasi TMDPDFs in coordinate space as function of $\lambda = zP^z$ with various m_π and P^z at $b_\perp = 3a$; right panels: comparison of original (data points) and extrapolated results (band).

As can be seen from right panels of Fig. 2, the fitted results (colored bands) agree with the original data points in the moderate λ region, and give smoothly-decaying distributions at large λ . The uncertainty from the extrapolation indicates that in momentum space the quasi TMDPDFs, which are defined as \hat{f}_Γ in Eq. 1, cannot be reliably predicted in the endpoint (conjugate to large λ) regions. It is consistent with LaMET power counting.

Together with the lattice result for Collins-Soper kernel [25] and intrinsic soft function [26], one can obtain numerical results for TMDPDFs. To obtain the physical TMDPDF, we extrapolate the pion mass to its physical value ($m_{\pi,\text{phy}} = 135\text{MeV}$) and P^z to infinity through the following ansatz [42]:

$$f_\Gamma(x, b_\perp, \mu, \zeta; m_\pi, P^z) = f_\Gamma(x, b_\perp, \mu, \zeta) \Big|_{\substack{m_\pi \rightarrow m_{\pi,\text{phy}} \\ P^z \rightarrow \infty}} \times \left[1 + d_0 (m_\pi^2 - m_{\pi,\text{phy}}^2) + \frac{d_1}{(P^z)^2} \right]. \quad (10)$$

Fig. 3 exhibits the x dependence of lattice data (last two subplots) and extrapolated TMDPDFs (first subplot) xf at $b_\perp = 3a$ and $\Gamma = \gamma^t$.

In the lattice simulation, both γ^t and γ^z can be used to reconstruct the quasi TMDPDFs since both of them approach the γ^+ in large momentum limit. It is anticipated that their deviations to the lightcone are proportional to $\mathcal{O}(M^2/(P^z)^2)$ with opposite signs. Thereby differences in results with these two Lorentz structures reflect power corrections when one applies operator product expansion for the quasi correlators. An interesting observation is that Ref. [43] found that the γ^t case has less operator

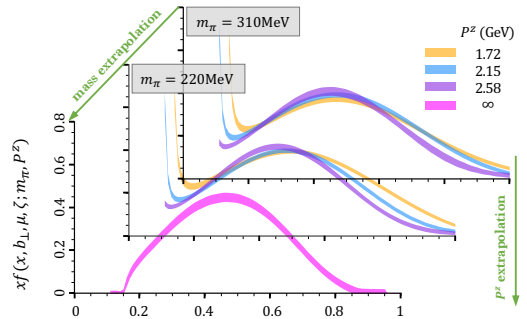


FIG. 3. Comparison of TMDPDFs before (six bands at last two subplots) and after (band at first subplot) extrapolation with $b_\perp = 3a$ and $\Gamma = \gamma^t$.

mixing effects. In order to illustrate the impact caused by different structures, we investigate a ratio

$$R \equiv \frac{f_{\gamma^t} - f_{\gamma^z}}{f_{\gamma^t} + f_{\gamma^z}}. \quad (11)$$

The upper panel in Fig. 4 shows the R value with m_π extrapolated to $m_{\pi,\text{phy}}$ at $\Gamma = \gamma^t$ and $b_\perp = 3a$. One can see that with the increase of nucleon momentum, the ratio R decreases, which indicates the suppression of power corrections. In the end-point regions, power corrections become larger, which again indicate the incapability of LaMET factorization in these regions. In our final results, we take the central value of R ($P^z = 2.58\text{GeV}$) as one source of systematic uncertainties.

Before drawing the conclusion, a most essential ingredient is to estimate the uncertainties. In addition

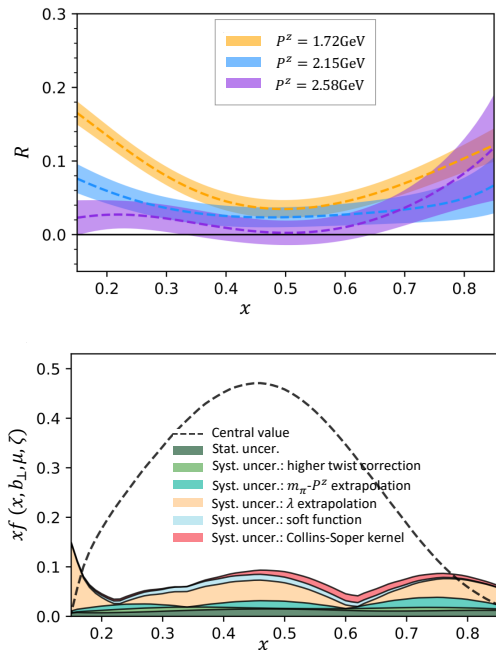


FIG. 4. Upper panel: R value with m_π extrapolated to $m_{\pi,\text{phy}}$ at $\Gamma = \gamma^t$ and $b_\perp = 3a$; lower panel: estimation of the statistic and systematic uncertainties, take $b_\perp = 3a$ as an example.

to statistical uncertainties that are already included, three main systematic uncertainties are considered in this work: the large- λ extrapolation, the $m_\pi - P_z$ joint extrapolation and residual power corrections. For the systematic uncertainty from large λ extrapolation, differences between the results with two fit ranges, $z \geq 8a$ and $z \geq 6a$, are used as an estimation. For the one from $m_\pi - P_z$ extrapolation, we take the deviation of the results with $m_\pi = 220$ MeV and $P^z = 2.58$ GeV from the extrapolated result. For the impact from the residual power corrections, central values of the R ratio at $P^z = 2.58$ GeV in the upper panel of Fig. 4 are employed as an estimation. In addition, we also include those uncertainties from the intrinsic soft function and Collins-Soper kernel [25, 26].

All these uncertainties to TMDPDFs with $b_\perp = 3a$, with the exception of power corrections and finite lattice spacing effect, are plotted in the lower panel of Fig. 4, with the central value shown as a comparison. The statistical uncertainty, illustrated by the dark green band, only contributes a small fraction to the total uncertainty, while systematic uncertainties play a more important role. Of all systematic uncertainties, the main contribution comes from the λ extrapolation as well as the uncertainties from soft function. The other contributions from $m_\pi - P_z$ extrapolation, the residual power corrections and Collins-Soper kernels, are similar in magnitude.

Combing all the known uncertainties, numerical results for the unpolarized TMDPDFs from lattice simulation

are shown as the colored bands in Fig. 5. The results are exhibited at the renormalization scale $\mu = 2$ GeV and rapidity scale $\sqrt{\zeta} = 2$ GeV. Phenomenological results [6–9] that are based on parameterizations and experimental inputs are also collected to provide a comparison with our results, shown as the different shaded bands in Fig. 5. Our results are in qualitative agreement with phenomenological results and share similar behaviors in b_\perp space: the central values slowly decrease and uncertainties are gradually increasing with the increase of b_\perp . From the figure, one can see that a peak exists in the x distribution, which corresponds to the largest probability of longitudinal momentum distributions of partons. However the peak positions are not exactly same for the lattice results and phenomenological results. The two shaded bands at the endpoint regions ($x < 0.2$ and $x > 0.8$) in each subplots of Fig. 5 indicate that LaMET predictions are not reliable there due to power corrections. Besides, since only one lattice spacing is used, the discretization uncertainties are not properly handled at this stage. Thereby the $b_\perp \sim a$ case might suffer sizable discretization effects.

Summary and Prospect: In summary, we have presented a first calculation of TMDPDFs inside a nucleon using LaMET expansion of the lattice data. The state-of-the-art techniques in renormalization and extrapolation on the lattice are adopted. One-loop contributions in the perturbative kernel are taken into account. We explored the dependence on pion mass and hadron momentum, and both statistical errors and systematic errors are included to give a reliable description of nucleons’ inner structure from the view of the parton distribution.

Though the final results are encouraging, there are improvements needed in the future, such as the simulations on a finer lattice, a high precision analysis with larger P^z , and larger transverse separations. On the theoretical side, more accurate perturbative contributions such as the two-loop corrections will also help improve the accuracy.

Acknowledgements: We thank Alessandro Bacchetta, Matteo Cerutti, Alexey Vladimirov for sharing their data for this work. We also thank the MILC collaboration for providing us their gauge configurations with dynamical fermions. This work is supported in part by Natural Science Foundation of China under grant No. 11735010, 11911530088, U2032102, 12005130, 12125503. The computations in this paper were run on the Siyuan-1 cluster supported by the Center for High Performance Computing at Shanghai Jiao Tong University, and Advanced Computing East China Sub-center. The numerical calculation in this study were also carried out on the ORISE Supercomputer, and HPC Cluster of ITP-CAS. X.J. and Y.S. are supported by the U.S. Department of Energy, Office of Science, Office of Nuclear Physics, under contract number DE-SC0020682. Y.Y. is supported in part by the Strategic Priority Research Program of Chinese

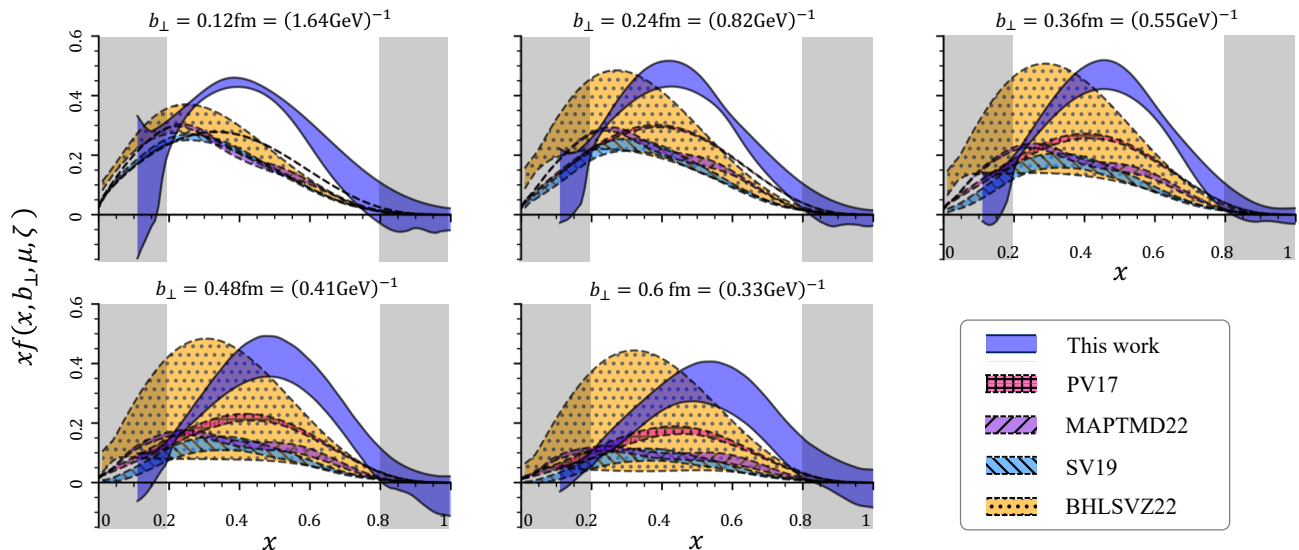


FIG. 5. Our final results for isovector unpolarized TMDPDFs $x f(x, b_{\perp}, \mu, \zeta)$ at renormalization scale $\mu = 2$ GeV and rapidity scale $\sqrt{\zeta} = 2$ GeV, extrapolated to physical pion mass 135 MeV and infinite momentum limit $P^z \rightarrow \infty$, compared with PV17 [6], MAPTMD22 [9], SV19 [7] and BHLSVZ22 [8] global fits (slashed bands). The colored bands denote our results with both statistical and systematic uncertainties, the shaded grey regions imply the endpoint regions where LaMET predictions are not reliable.

Academy of Sciences, Grant No. XDB34030303 and XDPB15. J.Z. is supported in part by National Natural Science Foundation of China under grant No. 11975051. A.S, W.W, Y.Y and J.Z are also supported by a NSFC-

DFG joint grant under grant No. 12061131006 and SCHA 458/22. Q.Z. is supported by the Key Laboratory of Particle Astrophysics and Cosmology, Ministry of Education of China.

SUPPLEMENTAL MATERIALS

Renormalization

In order to renormalize the bare quasi-TMD matrix elements, the square root of Wilson loop $\sqrt{Z_E}$ and logarithmic divergence factor Z_O need to be computed.

The Wilson loop $Z_E(r = 2L + z, b_{\perp}, a)$ is defined as the vacuum expectation of a rectangular shaped space-like gauge links with size $r \times b_{\perp}$. It is introduced to eliminate the linear divergence form as $e^{-\delta \bar{m} r}$, which comes from the self-energy corrections of the gauge link [28, 34], as well as the pinch-pole singularity, which comes from the heavy quark effective potential term $e^{-V(b_{\perp})L}$ from the interactions between the two Wilson lines along the z direction in the staple link [20]. In practice, the signal to noise ratio of $Z_E(r, b_{\perp}, a)$ grows fast and is hardly available at large r and/or b_{\perp} . To address this, we fit the effective energies of Wilson loop, which denote the QCD static potentials, and then extrapolate them at large r and/or b_{\perp} area, as in Ref. [27]. Numerical results of Wilson loop are shown in the upper panel of Fig. 6.

Besides, the logarithmic divergences factor Z_O can be extracted from the zero-momentum bare matrix elements $\tilde{h}_{\Gamma}^0(z, b_{\perp}, 0, a, L)$. In order to keep the renormalized matrix elements consistent with perturbation theory, Z_O should be determined with the condition:

$$Z_O(1/a, \mu, \Gamma) = \lim_{L \rightarrow \infty} \frac{\tilde{h}_{\Gamma}^0(z, b_{\perp}, 0, a, L)}{\sqrt{Z_E(2L + z, b_{\perp}, a)} \tilde{h}_{\Gamma}^{\overline{\text{MS}}}(z, b_{\perp}, \mu)} \quad (12)$$

in a specific window where $z \ll \Lambda_{\text{QCD}}^{-1}$ so that the perturbation theory works well. Here the perturbation results have been evolved from the intrinsic physical scale $2e^{-\gamma_E}/\sqrt{z^2 + b_{\perp}^2}$ to $\overline{\text{MS}}$ scale μ via renormalization group equation [44]. To preserve a good convergence of the perturbation theory before and after RG evolution, we choose the region where $b_{\perp} = a$, $z = 0$ or a . More discussions about RG evolution can be found in the following section. The numerical value for Z_O in this work is taken as 1.0622(87), of which the uncertainty is negligible compared with other systematic uncertainties.

With Eq. (12), it can be found that after dividing the bare matrix elements \tilde{h}_Γ^0 by $\sqrt{Z_E}$ and Z_O , the renormalized matrix elements we get should approximately equal to the RG evolved perturbation results $\tilde{h}_\Gamma^{\overline{\text{MS}}}$. The lower panel of Fig. 6 shows the consistency at points where we extract the Z_O factor, which serves as a check of the numerical result of Z_O .

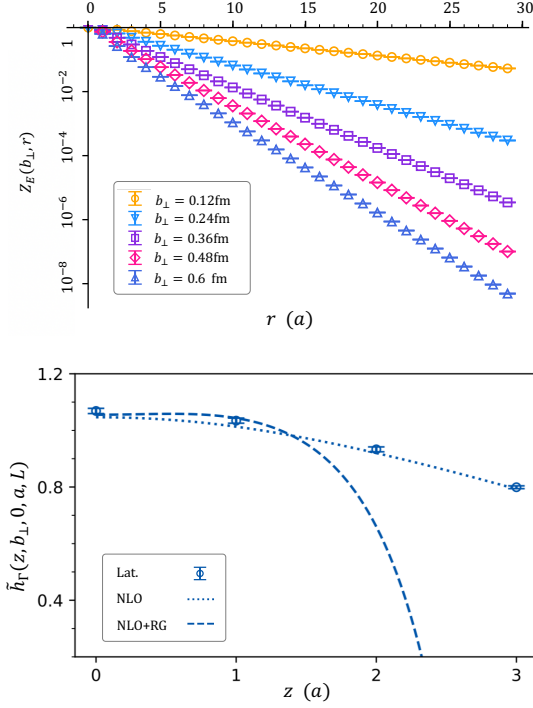


FIG. 6. Upper panel: Wilson loop with $r = 2L + z$. Lower panel: renormalized zero-momentum matrix element $\tilde{h}_\Gamma(z, b_\perp, 0, a, L)$ at $b_\perp = 1a$, compare with 1-loop results before and after and without RG resummation in $\overline{\text{MS}}$ scheme [44].

RG evolution of 1-loop matching kernel

The matching kernel H connecting quasi and light-cone TMDPDFs in LaMET factorization is defined as the exponential form: $H = e^h$, with 1-loop level result reads [20, 45]

$$h^{(1)}\left(\frac{\zeta_z}{\mu^2}\right) = \frac{\alpha_s C_F}{2\pi} \left(-2 + \frac{\pi^2}{12} + \ln \frac{\zeta_z}{\mu^2} - \frac{1}{2} \ln^2 \frac{\zeta_z}{\mu^2} \right), \quad (13)$$

where $\zeta_z = (2xP^z)^2$. The perturbative TMDPDFs usually performed in the $\overline{\text{MS}}$ scheme with a fixed renormalization scale μ , while the quasi TMDPDFs are associated with the Collins-Soper scale $\sqrt{\zeta_z}$, which is the intrinsic physical scale of the perturbative matching. In order

to expose the intrinsic physical scale [44], we resum the small momentum large logarithms $\sim \ln\left(\frac{\mu^2}{4x^2P^z}\right)$ through the renormalization group (RG) equation for H :

$$\mu^2 \frac{d}{d\mu^2} \ln H\left(\frac{\zeta_z}{\mu^2}\right) = \frac{1}{2} \Gamma_{\text{cusp}}(\alpha_s) \ln \frac{\zeta_z}{\mu^2} + \frac{\gamma_C(\alpha_s)}{2}, \quad (14)$$

where $\gamma_C = 2\gamma_F + \Gamma_S + 2\gamma_H$ with $\gamma_C^{(1)} = -C_F/\pi$ and $\gamma_C^{(2)} = (a_1 C_F C_A + a_2 C_F^2 + a_3 C_F n_f)$, the coefficients $a_1 = 44\zeta_3 - \frac{11\pi^2}{3} - \frac{1108}{27}$, $a_2 = -48\zeta_3 + \frac{28\pi^2}{3} - 8$ and $a_3 = \frac{2\pi^2}{3} + \frac{160}{27}$ [20, 45]. The cusp anomalous dimension Γ_{cusp} has been known up to four-loop level for the quark case [46, 47].

In practice, we employ the RG evolution starting from the Collins-Soper scale $\mu_0 = 2xP^z$ to $\mu = 2\text{GeV}$. After the resummation, the intrinsic scale $2xP^z$ appears in the running coupling $\alpha_s(2xP^z)$. Fig. 7 shows the comparison of 1-loop matching kernel with and without RG evolution. One can see that the RG evolution will revise the perturbative behavior at small- x region, and make the TMDPDFs prediction in this region to be less reliable.

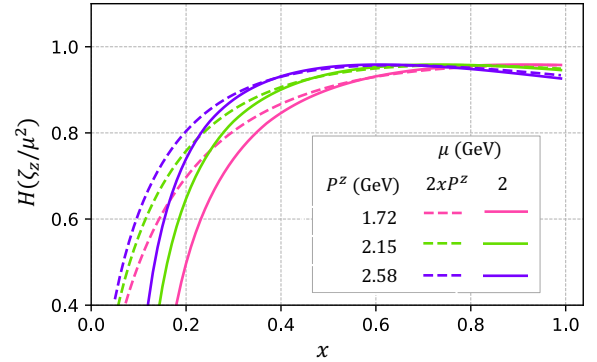


FIG. 7. Comparison of 1-loop matching kernel at Collins-Soper scale $\mu = 2xP^z$ (dashed lines) and $\overline{\text{MS}}$ scale $\mu = 2\text{GeV}$ (solid lines) with different P^z .

Fits of 2- and 3-point functions

As mentioned in the Lattice simulations section, we perform a full correlated joint fit combining two-point functions and the ratio defined in Eq. 8 to extract ground state matrix elements $\tilde{h}_\Gamma^0(z, b_\perp, P^z)$, the ΔE accounts for the excited state contamination. There are five values of the source-sink separation time in the range $t_{\text{seq}} \approx (0.48 - 0.84)$ fm in our fits, of which all contact points ($t = 0$ and $t = t_{\text{seq}}$) have been dropped. All these fits work well with $\chi^2/\text{d.o.f} \sim 1$ and p -value > 0.1 . For instance, as shown in Fig. 8, the posterior fit bands are well consistent with the data points at $\{z, b_\perp, P^z\} = \{3a, 1a, 16\pi/n_s\}$

and $\Gamma = \gamma^t$. The grey band denotes the extracted ground state matrix element with reasonable uncertainty.

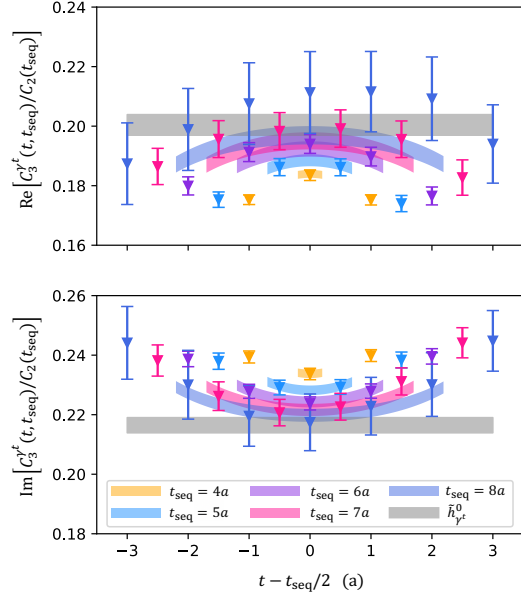


FIG. 8. Ratios of $C_3^{\gamma^t}(t, t_{\text{seq}})/C_2(t_{\text{seq}})$ (data points), as functions of t and t_{seq} , with $\{z, b_{\perp}, P^z\} = \{3a, 1a, 16\pi/n_s\}$ and $\Gamma = \gamma^t$, $m_{\pi} = 220\text{MeV}$. In this figure, the colored bands correspond to the fitted results, and the grey band reflects the ground-state contribution.

Quasi-TMDPDFs in momentum space

After extrapolation, one can Fourier-transform the renormalized quasi-TMDPDF correlations to momentum space

$$\tilde{f}_{\Gamma}(x, b_{\perp}, P^z, \mu) = \int \frac{dz}{2\pi} e^{-iz(xP^z)} \tilde{h}_{\Gamma}(z, b_{\perp}, P^z, \mu). \quad (15)$$

Results at $b_{\perp} = 3a$ with pion mass $m_{\pi} = 220\text{MeV}$ and $\Gamma = \gamma^t$ are shown in Fig. 9.

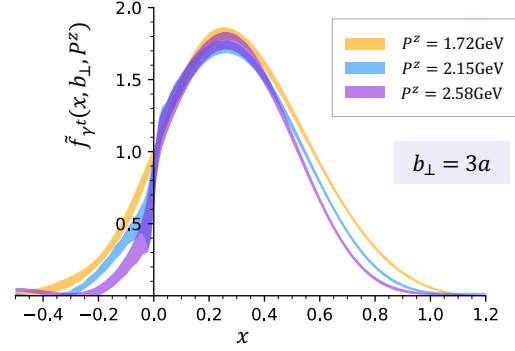


FIG. 9. The quasi TMDPDFs at momentum space with boosted momentum $P^z = \{1.72, 2.15, 2.58\}\text{GeV}$ at $b_{\perp} = 3a$ with $m_{\pi} = 220\text{MeV}$ and $\Gamma = \gamma^t$.

- doi:10.5506/APhysPolB.46.2501 [arXiv:1507.05267 [hep-ph]].
- [3] J. C. Collins, D. E. Soper and G. F. Sterman, Nucl. Phys. B **250**, 199-224 (1985) doi:10.1016/0550-3213(85)90479-1
- [4] A. Accardi, J. L. Albacete, M. Anselmino, N. Armesto, E. C. Aschenauer, A. Bacchetta, D. Boer, W. K. Brooks, T. Burton and N. B. Chang, *et al.* Eur. Phys. J. A **52**, no.9, 268 (2016) doi:10.1140/epja/i2016-16268-9 [arXiv:1212.1701 [nucl-ex]].
- [5] I. Moutl, H. X. Zhu and Y. J. Zhu, JHEP **08**, 280 (2022) doi:10.1007/JHEP08(2022)280 [arXiv:2205.02249 [hep-ph]].
- [6] A. Bacchetta, F. Delcarro, C. Pisano, M. Radici and A. Signori, JHEP **06**, 081 (2017) [erratum: JHEP **06**, 051 (2019)] doi:10.1007/JHEP06(2017)081 [arXiv:1703.10157 [hep-ph]].
- [7] I. Scimemi and A. Vladimirov, JHEP **06**, 137 (2020) doi:10.1007/JHEP06(2020)137 [arXiv:1912.06532 [hep-ph]].
- [8] M. Bury, F. Hautmann, S. Leal-Gomez, I. Scimemi, A. Vladimirov and P. Zurita, JHEP **10**, 118 (2022) doi:10.1007/JHEP10(2022)118 [arXiv:2201.07114 [hep-ph]].
- [9] A. Bacchetta *et al.* [WMAP], JHEP **10**, 127 (2022) doi:10.1007/JHEP10(2022)127 [arXiv:2206.07598 [hep-ph]].
- [10] P. Hagler, B. U. Musch, J. W. Negele and A. Schafer, EPL **88**, no.6, 61001 (2009) doi:10.1209/0295-5075/88/61001 [arXiv:0908.1283 [hep-lat]].
- [11] B. U. Musch, P. Hagler, M. Engelhardt, J. W. Negele and A. Schafer, Phys. Rev. D **85**, 094510 (2012) doi:10.1103/PhysRevD.85.094510 [arXiv:1111.4249 [hep-lat]].
- [12] B. Yoon, T. Bhattacharya, M. Engelhardt, J. Green, R. Gupta, P. Hägler, B. Musch, J. Negele, A. Pochinsky and S. Syritsyn, [arXiv:1601.05717 [hep-lat]].
- [13] B. Yoon, M. Engelhardt, R. Gupta, T. Bhattacharya, J. R. Green, B. U. Musch, J. W. Negele, A. V. Pochinsky, A. Schäfer and S. N. Syritsyn, Phys. Rev. D **96**, no.9, 094508 (2017) doi:10.1103/PhysRevD.96.094508 [arXiv:1706.03406 [hep-lat]].
- [14] X. Ji, Phys. Rev. Lett. **110**, 262002 (2013) doi:10.1103/PhysRevLett.110.262002 [arXiv:1305.1539

* Corresponding author: wei.wang@sjtu.edu.cn

† Corresponding author: zhangqa@buaa.edu.cn

- [1] J. C. Collins and D. E. Soper, Nucl. Phys. B **193**, 381 (1981) [erratum: Nucl. Phys. B **213**, 545 (1983)] doi:10.1016/0550-3213(81)90339-4
- [2] R. Angeles-Martinez, A. Bacchetta, I. I. Balitsky, D. Boer, M. Boglione, R. Boussarie, F. A. Ceccopieri, I. O. Cherednikov, P. Connor and M. G. Echevarria, *et al.* Acta Phys. Polon. B **46**, no.12, 2501-2534 (2015)

- [hep-ph]].
- [15] X. Ji, *Sci. China Phys. Mech. Astron.* **57**, 1407-1412 (2014) doi:10.1007/s11433-014-5492-3 [arXiv:1404.6680 [hep-ph]].
- [16] X. Ji, P. Sun, X. Xiong and F. Yuan, *Phys. Rev. D* **91**, 074009 (2015) doi:10.1103/PhysRevD.91.074009 [arXiv:1405.7640 [hep-ph]].
- [17] X. Ji, Y. Liu and Y. S. Liu, *Nucl. Phys. B* **955**, 115054 (2020) doi:10.1016/j.nuclphysb.2020.115054 [arXiv:1910.11415 [hep-ph]].
- [18] M. A. Ebert, I. W. Stewart and Y. Zhao, *JHEP* **09**, 037 (2019) doi:10.1007/JHEP09(2019)037 [arXiv:1901.03685 [hep-ph]].
- [19] P. Shanahan, M. Wagman and Y. Zhao, *Phys. Rev. D* **102**, no.1, 014511 (2020) doi:10.1103/PhysRevD.102.014511 [arXiv:2003.06063 [hep-lat]].
- [20] X. Ji, Y. Liu and Y. S. Liu, *Phys. Lett. B* **811**, 135946 (2020) doi:10.1016/j.physletb.2020.135946 [arXiv:1911.03840 [hep-ph]].
- [21] X. Ji and Y. Liu, *Phys. Rev. D* **105**, no.7, 076014 (2022) doi:10.1103/PhysRevD.105.076014 [arXiv:2106.05310 [hep-ph]].
- [22] M. Schlemmer, A. Vladimirov, C. Zimmermann, M. Engelhardt and A. Schäfer, *JHEP* **08**, 004 (2021) doi:10.1007/JHEP08(2021)004 [arXiv:2103.16991 [hep-lat]].
- [23] Q. A. Zhang *et al.* [Lattice Parton], *Phys. Rev. Lett.* **125**, no.19, 192001 (2020) doi:10.22323/1.396.0477 [arXiv:2005.14572 [hep-lat]].
- [24] Y. Li, S. C. Xia, C. Alexandrou, K. Cichy, M. Constantinou, X. Feng, K. Hadjiyiannakou, K. Jansen, C. Liu and A. Scapellato, *et al.* *Phys. Rev. Lett.* **128**, no.6, 062002 (2022) doi:10.1103/PhysRevLett.128.062002 [arXiv:2106.13027 [hep-lat]].
- [25] M. H. Chu *et al.* [LPC], *Phys. Rev. D* **106**, no.3, 034509 (2022) doi:10.1103/PhysRevD.106.034509 [arXiv:2204.00200 [hep-lat]].
- [26] M. H. Chu *et al.* [Lattice Parton Collaboration (LPC)], in preparation.
- [27] K. Zhang *et al.* [[Lattice Parton Collaboration (LPC)]], *Phys. Rev. Lett.* **129**, no.8, 082002 (2022) doi:10.1103/PhysRevLett.129.082002 [arXiv:2205.13402 [hep-lat]].
- [28] X. Ji, J. H. Zhang and Y. Zhao, *Phys. Rev. Lett.* **120**, no.11, 112001 (2018) doi:10.1103/PhysRevLett.120.112001 [arXiv:1706.08962 [hep-ph]].
- [29] T. Ishikawa, Y. Q. Ma, J. W. Qiu and S. Yoshida, *Phys. Rev. D* **96**, no.9, 094019 (2017) doi:10.1103/PhysRevD.96.094019 [arXiv:1707.03107 [hep-ph]].
- [30] J. Green, K. Jansen and F. Steffens, *Phys. Rev. Lett.* **121**, no.2, 022004 (2018) doi:10.1103/PhysRevLett.121.022004 [arXiv:1707.07152 [hep-lat]].
- [31] X. Ji, Y. Liu, A. Schäfer, W. Wang, Y. B. Yang, J. H. Zhang and Y. Zhao, *Nucl. Phys. B* **964**, 115311 (2021) doi:10.1016/j.nuclphysb.2021.115311 [arXiv:2008.03886 [hep-ph]].
- [32] P. Shanahan, M. L. Wagman and Y. Zhao, *Phys. Rev. D* **101**, no.7, 074505 (2020) doi:10.1103/PhysRevD.101.074505 [arXiv:1911.00800 [hep-lat]].
- [33] X. D. Ji and M. J. Musolf, *Phys. Lett. B* **257**, 409-413 (1991) doi:10.1016/0370-2693(91)91916-J
- [34] Y. K. Huo *et al.* [Lattice Parton Collaboration (LPC)], *Nucl. Phys. B* **969**, 115443 (2021) doi:10.1016/j.nuclphysb.2021.115443 [arXiv:2103.02965 [hep-lat]].
- [35] Y. Ji, J. H. Zhang, S. Zhao and R. Zhu, *Phys. Rev. D* **104**, no.9, 094510 (2021) doi:10.1103/PhysRevD.104.094510 [arXiv:2104.13345 [hep-ph]].
- [36] Supplemental materials, for the details of the renormalization, RG evolution of 1-loop matching kernel, correlation function fit and quasi-TMDPDFs in momentum space.
- [37] M. A. Ebert, S. T. Schindler, I. W. Stewart and Y. Zhao, *JHEP* **04**, 178 (2022) doi:10.1007/JHEP04(2022)178 [arXiv:2201.08401 [hep-ph]].
- [38] A. Hasenfratz and F. Knechtli, *Phys. Rev. D* **64**, 034504 (2001) doi:10.1103/PhysRevD.64.034504 [arXiv:hep-lat/0103029 [hep-lat]].
- [39] A. Bazavov *et al.* [MILC], *Phys. Rev. D* **87**, no.5, 054505 (2013) doi:10.1103/PhysRevD.87.054505 [arXiv:1212.4768 [hep-lat]].
- [40] G. S. Bali, B. Lang, B. U. Musch and A. Schäfer, *Phys. Rev. D* **93**, no.9, 094515 (2016) doi:10.1103/PhysRevD.93.094515 [arXiv:1602.05525 [hep-lat]].
- [41] G. W. Kilcup, S. R. Sharpe, R. Gupta, G. Guralnik, A. Patel and T. Warnock, *Phys. Lett. B* **164**, 347-355 (1985) doi:10.1016/0370-2693(85)90339-9
- [42] H. W. Lin, J. W. Chen and R. Zhang, [arXiv:2011.14971 [hep-lat]].
- [43] M. Constantinou, H. Panagopoulos and G. Spanoudes, *Phys. Rev. D* **99**, no.7, 074508 (2019) doi:10.1103/PhysRevD.99.074508 [arXiv:1901.03862 [hep-lat]].
- [44] Y. Su, J. Holligan, X. Ji, F. Yao, J. H. Zhang and R. Zhang, [arXiv:2209.01236 [hep-ph]].
- [45] X. Ji, Y. S. Liu, Y. Liu, J. H. Zhang and Y. Zhao, *Rev. Mod. Phys.* **93**, no.3, 035005 (2021) doi:10.1103/RevModPhys.93.035005 [arXiv:2004.03543 [hep-ph]].
- [46] S. Moch, B. Ruijl, T. Ueda, J. A. M. Vermaseren and A. Vogt, *JHEP* **10**, 041 (2017) doi:10.1007/JHEP10(2017)041 [arXiv:1707.08315 [hep-ph]].
- [47] R. N. Lee, A. V. Smirnov, V. A. Smirnov and M. Steinhauser, *JHEP* **02**, 172 (2019) doi:10.1007/JHEP02(2019)172 [arXiv:1901.02898 [hep-ph]].